Cytometry PART A
Journal of the International Society for Advancement of Cytometry

Quantitative Performance Evaluation of a Back-Illuminated sCMOS Camera with 95% QE for Super-Resolution Localization Microscopy

Yujie Wang,[1,2†] Lingxi Zhao,[1,2†] Zhe Hu,[1,2†] Yina Wang,[1,2] Zeyu Zhao,[1,2] Luchang Li,[1,2] Zhen-Li Huang[1,2*]

[1]Britton Chance Center for Biomedical Photonics, Wuhan National Laboratory for Optoelectronics-Huazhong University of Science and Technology, Wuhan 430074, China

[2]MoE Key Laboratory for Biomedical Photonics, Collaborative Innovation Center for Biomedical Engineering, School of Engineering Sciences, Huazhong University of Science and Technology, Wuhan, Hubei 430074, China

Received 18 July 2017; Revised 29 September 2017; Accepted 18 October 2017

*Correspondence to: Zhen-Li Huang, Britton Chance Center for Biomedical Photonics, Wuhan National Laboratory for Optoelectronics-Huazhong University of Science and Technology, Wuhan 430074, China. Email: leo@mail.hust.edu.cn

†These authors contributed equally to this work

Published online 22 November 2017 in Wiley Online Library (wileyonlinelibrary.com)

DOI: 10.1002/cyto.a.23282

Abstract

Scientific Complementary Metal Oxide Semiconductor (sCMOS) cameras were introduced into the market in 2009 and are now becoming a major type of commercial cameras for low-light imaging. sCMOS cameras provide simultaneously low read noise, high readout speed, and large pixel array; however, the relatively low quantum efficiency (QE) of sCMOS cameras has been a major limitation for its application in single molecule imaging, especially super-resolution localization microscopy which requires high detection sensitivity. Here we report the imaging performance of a newly released back-illuminated sCMOS camera (called Dhyana 95 from Tucsen) which is claimed to be the world's first 95% QE sCMOS camera. The imaging performance evaluation is based on a new methodology which is designed to provide paired images from two tested cameras under almost identical experimental conditions. We verified that this new 95% QE sCMOS camera is able to provide superior imaging performance over a representative front-illuminated sCMOS camera (Hamamatsu Flash 4.0 V2) and a popular back-illuminated EMCCD camera (Andor iXon 897 Ultra) in a wide signal range. We hope this study will inspire more studies on using sCMOS cameras in super-resolution localization microscopy, or even single molecule imaging. © 2017 International Society for Advancement of Cytometry

Key terms

fluorescence; single-molecule studies; superresolution localization microscopy; low-light camera; sCMOS camera

Ever since its birth, super-resolution localization microscopy (SRLM), including photoactivated localization microscopy (PALM) (1), fluorescence photoactivated localization microscopy (FPALM) (2), stochastic optical reconstruction microscopy (STORM) (3), direct stochastic optical reconstruction microscopy (dSTORM) (4) and many others, has been an important tool for biology because it brings the spatial resolution of optical microscopy down to the nanoscale through a relative simple setup. The remarkable improvement in the spatial resolution of SRLM relies on mainly three steps: controlling single molecule fluorescence by photoswitching or photoactivation, detecting the fluorescence from isolated molecules by a low-light camera, and subsequently determining the molecule positions by a proper localization algorithm. Clearly, the performance of low-light cameras determines the quality of single molecule imaging and thus the localization results (5–8). Therefore, the selection of a suitable low-light camera is undoubtedly critical for constructing a localization microscope and achieving ultimate localization performance.

ISAC International Society for Advancement of Cytometry

Commercial low-light cameras are mainly from three camera technologies: charge-coupled device (CCD) cameras, electron multiplying CCD (EMCCD) cameras, and complementary metal oxide semiconductor (CMOS) cameras. Generally, a low-light camera consists of an array of pixels, and multiple signal conversion steps are required to present a final digital image (9). Specifically, for a CCD camera, incident signal photons hitting a pixel of a low-light camera are firstly converted to photoelectrons (unit: e–) using the image sensor inside the camera. Here, the signal intensity is usually described with the amount of photons per pixel (ph/px), and the photon-electron conversion efficiency is called quantum efficiency (QE). The QE value varies from 0% to 100%. Then, the photoelectrons are converted into a voltage, amplified, and then converted into a digital number (DN) using multiple electronic components in the camera. Shot noise (unit: e–) is the major noise source during the photo-electron conversion process, while read noise is a combination of system noises raising from the process of converting photoelectrons into a digital number. Read noise is usually described as the standard deviation of electron number from a series of images. Generally, we use root mean square (rms), and median of these standard deviation values to quantify a camera's read noise.

There is a tradeoff between image readout speed and read noise. To provide low read noise at higher imaging speeds, EMCCD cameras introduce an additional electron multiplication (EM) register to conventional CCD cameras. This EM register multiplies the photoelectrons before converting them to a voltage (9). Hence, EMCCD cameras provide not only ultra-low read noise ($<$ 1 e– with EM gain) at high readout rate (10∼20 MHz @14-bit), but also ultimate quantum efficiency (QE, up to 97%). Unfortunately, the EM register introduces an additional noise called excess noise (9,10).

In SRLM, EMCCD cameras have been widely considered as optimal low-light cameras for detecting the weak fluorescence from single molecules. However, starting from 2009, a new type of low-light cameras called scientific CMOS (sCMOS) cameras, has been actively explored as an alternative to the popular EMCCD cameras in SRLM (10–15), because sCMOS cameras offer not only low read noise (1 $\sim$ 2 e–) at extremely high readout rate (400–500 MHz @16-bit), but also at least 10 times larger pixel array than that from EMCCD cameras. However, comparing to EMCCD cameras which provide high QE, most sCMOS cameras have a relatively low QE (70–80% maximum) due to the front-illuminated technology, and thus present a weaker detected signal in single molecule fluorescence images. Therefore, currently the relatively low QE of sCMOS cameras is the major reason which limits the power and versatility of sCMOS cameras in single molecule imaging applications, including but not limited to SRLM.

Fortunately, the first back-illuminated sCMOS image sensor called GSENSE400BSI was invented in April 2015 by Gpixel Inc (Changchun, China). About one year later, an updated version of this sensor, GSENSE400BSI-TVISB, was used to produce a back-illuminated sCMOS camera (Dhyana 95) by a company called Tucsen (Fuzhou, China). This camera was claimed to provide an ultimate QE (95%), along with other attractive specifications: low read noise (1.71 e– median), fast readout rate (∼101 MHz @16-bit), and large pixel array (2048 $\times$ 2048 pixels). Shortly after the invention of Dhyana 95, Photometrics (USA) announced Prime 95B, another back-illuminated sCMOS camera which was based on the same sensor chip as Dhyana 95. Comparing to Dhyana 95, Prime 95B provides similar read noise (1.3 e– median) and read out rate (118 MHz @ 12-bit, or 59 MHz @ 16-bit), but with a smaller pixel array (1200 $\times$ 1200 pixels). Theoretically, after considering the ultimate QE and the low read noise, both Dhyana 95 and Prime 95B are expected to provide similar detection sensitivity and exhibit better imaging performance than their front-illuminated predecessor (for example, Hamamatsu Flash 4.0 V2 or Andor Zyla 4.0), and eventually would attract more researchers to use sCMOS cameras in SRLM (16–22). However, the imaging performance of the newly released back-illuminated sCMOS cameras in single molecule imaging or SRLM still remains to be evaluated.

In this article, we evaluated the imaging performance of a newly released back-illuminated sCMOS camera (Tucsen Dhyana 95) with maximum QE of 95%. This evaluation is based on a new methodology which is suitable for direct comparison of two cameras with close imaging performance. We found that this back-illuminated sCMOS camera presents a competitive advantage over a popular front-illuminated sCMOS camera (Hamamatsu Flash 4.0 V2) or a typical back-illuminated EMCCD camera (Andor iXon 897 Ultra) in super-resolution localization microscopy in a wide signal range.

Materials and Methods

Optical Setup for Direct Comparison of Two Low-Light Cameras

The optical setup for direct camera comparison is based on an Olympus IX 71 inverted optical microscope and is shown in Figure 1. The excitation source is a 640 nm diode-pumped solid-state laser (CNILaser, China). The duration of laser irradiance is controlled by an electronic shutter. The laser intensity is adjusted by a neutral density (ND) filter. The laser beam is expanded by a telescope consisting of lenses L1 and L2, guided by aluminum mirrors (M1–M4), and focused by a lens (L3) into an Olympus 100X/NA1.4 oil immersion objective. The emitted light from the sample is firstly collected with the same objective, passes through a dichroic mirror (DM), is filtered with a band-pass filter (EF), and is focused by a tube lens (L4). Then, the fluorescence beam is collimated by L5 (f = 150 mm) and separated equally by a 50:50 beam splitter (BS). Finally, the transmitted fluorescence beam is focused onto Camera 1 (Hamamatsu ORCA-Flash 4.0 V2, pixel size: 6.5 μm, SN: 750939 or Andor iXon 897 Ultra, pixel size: 16 μm, SN: X-4652) with lens L6 (f = 100 mm, 250 mm, respectively), while the reflected fluorescence beam is focused onto Camera 2 (Tucsen Dhyana 95, pixel size: 11 μm, SN: KBS4951607001) with lens L7 (f = 180 mm). An external trigger is used to synchronize the exposure times of the two cameras. We note that the optics in the detection path was

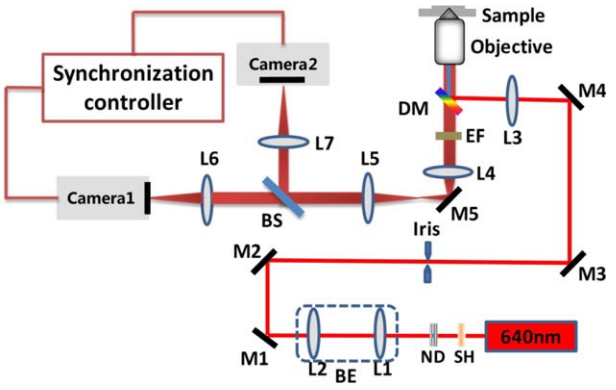

Figure 1. The optical setup for direct experimental comparison of two low-light cameras. SH: Electronic Shutter (UNIBLITZ VS14, Vincent Associates); ND: Neutral density filters; BE: Beam expander; L1-L7: Achromatic lens; L1: $f = 38.1$ mm; L2: $f = 200$ mm; L3: $f = 250$ mm; L4: Tube lens from Olympus; L5: $f = 150$ mm; L6: $f = 100$ mm/250 mm; L7: $f = 180$ mm; M1-M4: Aluminum mirrors; M5: 100% reflected prism (Olympus); DM: Dichroic mirror (z660dcxr, Chroma); EF: Emission filter (ET 700/70, Chroma); BS: 50:50 Broadband plate beam splitter (BSW16, Thorlabs); Camera 1: Hamamatsu ORCA-Flash4.0 V2/Andor iXon 897 Ultra; Camera 2: Tucsen Dhyana 95; Objective: Olympus UPLSAPO100XO,100X/NA1.4. Note that the lens pair L5/L7 (or L5/L6) provides a secondary magnification to match the pixel size at sample plane. [Color figure can be viewed at wileyonlinelibrary.com]

designed delicately to ensure that the splitting ratio is close to 1:1 and the pixel size at sample plane for both cameras is matched (close to 100 nm). Other information related to the setup is shown in the legend of Figure 1.

Sample Preparation and Image Acquisition

Sample preparation and image acquisition were mainly described in our previous work (10). Fluorescent beads were used as the sample, because they can provide controllable emitted intensity with negligible photobleaching. Briefly, to obtain a sample with stationary fluorescence, a drop of aqueous suspension of 200 nm fluorescent beads (F8807, FluoSpheres, Molecular Probes) was deposited onto a specimen slide and allowed to evaporate. The dried fluorescence beads were embedded in immersion oil to match refractive index and then sealed with a cover slip and nail polish. Note that the beads with large size were chosen to obtain highly stable fluorescence. During image acquisition, the signal brightness from the beads was controlled by laser intensity, while uniform photon background with different intensity levels was added to the images using the microscope's halogen lamp. Under certain signal and background levels, a set of 2000 successive image frames was captured using the optical setup described in Figure 1. The exposure time for both cameras was controlled to be the same (25 ms) for all measurements. Note that the background levels in this study were calculated from uniform areas far away from the fluorescence signal.

For comparing the imaging performance in biological samples, COS-7 cells were fixed with 3% paraformaldehyde, 0.05% glutaraldehyde and 0.2% Triton X-100 in PBS. After being washed with PBS, the cells were blocked with 3% BSA and 0.2% Triton X-100 in PBS for 1 h, and then stained with mouse monoclonal anti–α-tubulin antibody (Sigma T5168, 2 μg/ml) for 1.5 h. The cells were then washed with PBS and then stained with Alexa Fluor 647 goat anti-mouse IgG (Abcam ab150119, 4 μg/ml) for 1 h. The cells were washed with PBS, and then soaked in STORM buffer (6). The STORM experiments were performed on the optical setup described in "Optical Setup for Direct Comparison of Two Low-Light Cameras" Section, and the exposure time was set to be 20 ms.

Defining and Calculating Localization Precision

Localization precision is a key metric for benchmarking the imaging performance for localization microscopy. According to the literature (15,17), we define localization precision from the statistical positions of a stationary emitter under repeated imaging (see Fig. 2). We calculate localization precision as $\sigma = \sqrt{\sigma_x^2 + \sigma_y^2}$, where σ_x and σ_y represent the standard deviation of the center positions in x and y dimension, respectively. The calculation process of localization precision is similar to our previous work (10).

To estimate the measurement error for localization precision, we divide equally a whole dataset (2000 frames) into 40 subsets (that is, 50 frames per subset), and calculate the localization precision values for each subset. Then, the localization precision values from all 40 subsets are used to calculate the mean value and the standard deviation of the localization precision of the whole dataset. Another benefit arisen from this treatment is that the impact of stage drift (brought by platform vibration, thermal drift, etc.) on localization precision is considerably weakened by division of the whole dataset. Meanwhile, we carefully monitor the stage drift inside all raw images and remove large stage drift before any further calculation on localization precision.

Quantifying Read Noise and Relative Signal-Noise-Ratio

In order to better quantify the noise sources of cameras, we conduct a photon transfer curve (PTC) measurement (9,23) to statistically characterize a camera's response to illumination. The PTC measurement is based on our previous

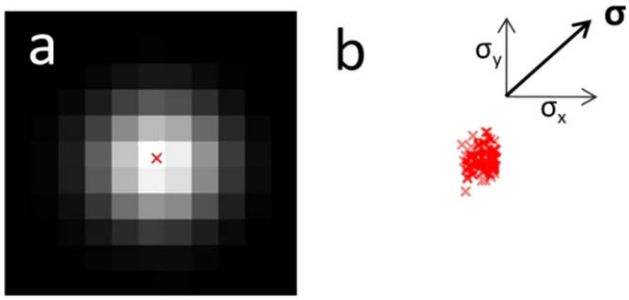

Figure 2. Defining localization precision from repeated imaging of a stationary emitter. (**a**) The PSF of the emitter and its center position (red cross) found by a suitable localization algorithm. (**b**) Distribution of the center positions of the emitter from repeated imaging. The localization precision (σ) is calculated from the square root of the sum of variance of the center position distributions in x and y dimensions. [Color figure can be viewed at wileyonlinelibrary.com]

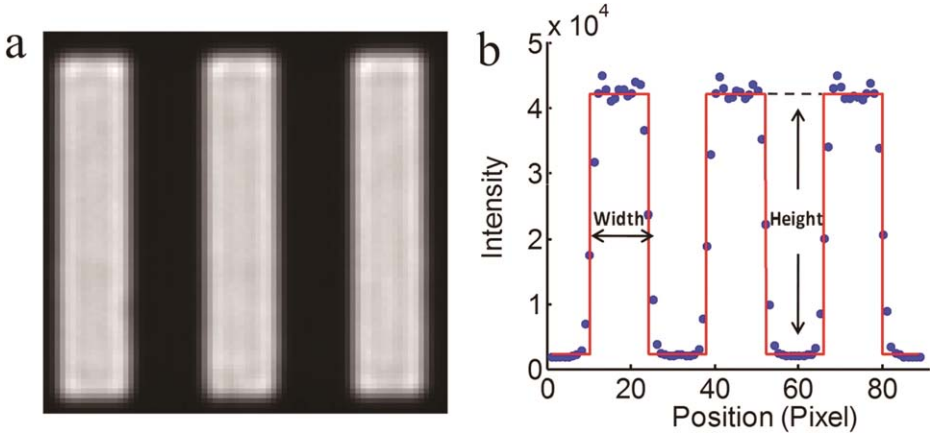

Figure 3. Characterizing the beam splitting ratio and the pixel size at sample plane. (**a**) An averaged bright field image from a 1951 USAF resolution target (Group 7, Element 2; The bar width: 3.47 μm), which was captured by a 40X objective and detected by a Hamamatsu ORCA-Flash 4.0 V2 sCMOS camera; (**b**) the projected intensity distribution of (a) to the horizontal direction (blue dots) and the fitted curve with rectangular function (red line). The width and the height of the bars in the fitted curve were used to calculate the beam splitting ratio and the total magnification of the optical setup, respectively. [Color figure can be viewed at wileyonlinelibrary.com]

article (10), with some modifications in the optics to ensure uniform illumination according to the EMVA 1288 standard release 3.1 (24). Here is a simple explanation of how the measurement is conducted, and more details and advantages of rSNR utilization are in our previous article. For each incident signal levels (S), thousands of frames are acquired under uniform illumination, and total noise (Ntot) is obtained. S represents the mean incident photon, and Ntot stands for the standard deviation of the signal. Specially, when the incident photon is equal to zero (when camera is placed in darkness), the temporal standard deviation is equal to read noise. While it is conventional to quantify sensitivity and image quality by plotting the SNR versus incident signal levels, we characterize camera performance with relative signal-noise-ratio (rSNR) in order to separate camera-induced noises from photon shot noise (10). The meaning of rSNR is the relative SNR of a real camera to the SNR of a hypothetically perfect camera. The SNR of a real camera is thus calculated by: SNRreal = S/Ntot. The SNR for a hypothetical perfect camera with only shot noise is: SNRperfect = sqrt(S). We define relative SNR: rSNR = SNRreal/SNRperfect.

Results

System Calibration

Calibrating camera sensitivity. To quantify the camera sensitivity difference and improve the accuracy in the light intensity measurement, we measured experimentally the responses of the two cameras to the same incident light intensities which were monitored by another camera (Hamamatsu ORCA-Flash 4.0 V2, pixel size: 6.5 μm, SN: 740888, hereafter called calibration camera). The calibration camera was placed on the left port of an Olympus IX 71 inverted microscope, while one of the test cameras (the Tucsen Dhyana 95, Hamamatsu Flash 4.0 V2, or Andor iXon 897 Ultra cameras in this study) was placed on the right port. Bright field images from a 1951 USAF resolution target were collected by an Olympus 40X/NA0.95 dry objective and captured by the calibration camera in the left port and then the test camera in the right port. The incident light intensity was changed to cover the dynamic range of the test camera, and 1000 frames of images were acquired and then averaged for each incident signal level. By calculating the total photon number of incident signal (after offset subtraction) from a resolution bar in the 1951 USAF resolution target, the relative sensitivity of the test camera to the calibration camera was obtained. The measurement was performed independently for at least three times, and all of the test cameras were quantified separately.

The relative sensitivity ratio between the Tucsen Dhyana 95 camera and the Hamamatsu Flash 4.0 V2 camera is found to be 1.35:1. The relative sensitivity ratio between the Andor iXon 897 Ultra camera and the Hamamatsu Flash 4.0 V2 camera is found to be 0.8333:1. The relative camera sensitivity difference in all of the test cameras was compensated in the further studies.

The splitting ratio and the pixel size at the sample plane. We used a 1951 USAF resolution target to characterize the beam splitting ratio and the pixel size at the sample plane in our optical setup. A total of 100 frames of bright field images from the target was collected by an Olympus 40X/NA0.95 dry objective and detected simultaneously by the new 95% sCMOS camera (Tucsen Dhyana 95) and one of the common cameras (Hamamatsu Flash 4.0 V2 or Andor iXon 897 Ultra). The images from each camera were averaged (see Fig. 3a for an example), projected to the horizontal dimension, and fitted with rectangular function (Fig. 3b). The beam splitting ratio was calculated by the ratio of the fitted bar areas (the product of the bar width and the bar height) from the two cameras, while the total magnification of the optical setup can be found by dividing the fitted bar width (the product of the number of pixels and the pixel size of the sensor) with the actual bar width (provided by the manufacturer of the resolution target).

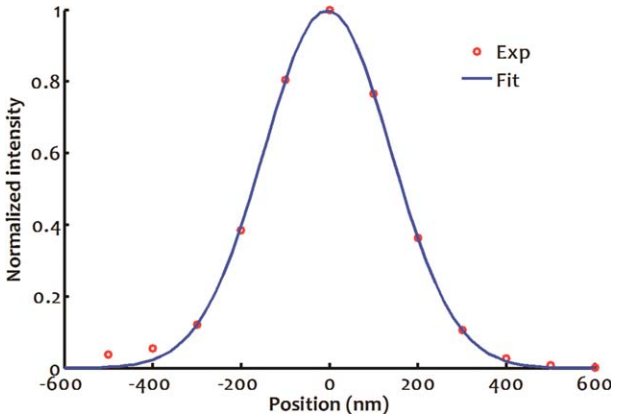

Figure 4. Characterizing the PSF of the optical setup. The experimental data (red circles) from an overlaid image from several 200 nm fluorescent beads were fitted with Gaussian function (blue curve). The fitted curve was found to have FWHM of 338 nm, and standard deviation of 143 nm. [Color figure can be viewed at wileyonlinelibrary.com]

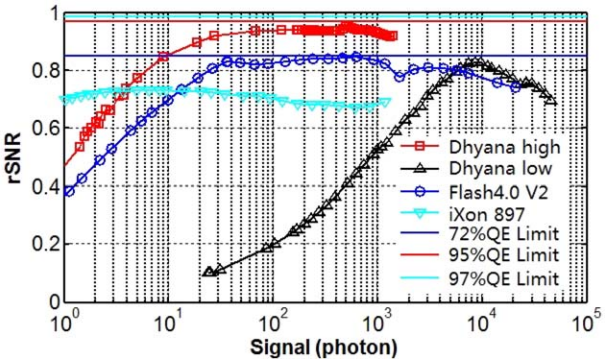

Figure 5. The rSNR curves of the test cameras in this study. Tucsen Dhyana 95 in high gain mode (red squares) and low gain mode (black triangles), Hamamatsu Flash 4.0 V2 (blue dots), Andor iXon 897 Ultra (cyan triangles) with EM gain of 100 and readout speed of 10 MHz. The rSNR curves for shot-noise-limited cameras with different QE were also shown here. The experiments were measured with 594 ± 20 nm incident light. [Color figure can be viewed at wileyonlinelibrary.com]

Note that the total magnification is the product of the magnification of the objective and the secondary magnification (see Fig. 1), and the pixel size at sample plane can be obtained by dividing the pixel size of the sensor by the total magnification.

From five independent measurements, the mean beam splitting ratio (Camera 1: Camera 2) was calculated to be (0.92 ± 0.01):1, while the pixel size at the sample plane for both cameras were calculated to be very close to the following theoretical values: 6.5 μm/(100 × 100/150) = 97.50 nm (for the Flash 4.0 V2), 11 μm/(100 × 180/150) = 91.67 nm (for the Dhyana 95), and 16 μm/(100 × 250/150) = 96.00 nm (for the iXon 897 Ultra).

The point spread function. Using the fluorescence images from fluorescent beads, we characterized the point spread function (PSF) of our optical setup shown in Figure 1. We found that the fluorescence images from 200 nm fluorescent beads spread over 7 × 7 pixels, where the amplitude of Gaussian function occupies ~7.3% of the total incident signal in our system. We overlaid 500 successive images to generate an averaged PSF image. Then, the averaged image was projected to the horizontal direction. Finally, the obtained intensity profile was fitted by Gaussian function. The full-width-at-half-maximum (FWHM) of the PSF was found to be 338 nm (Fig. 4). Based on seven beads in two thousand images, the FWHM of PSF is found to be 331 ± 7 nm. For comparison, the PSF of 20 nm (F8783, FluoSpheres, Molecular Probes) and 200 nm beads sealed in cover slip without immersion oil were also measured, and the FWHM values from both samples were found to be 353 nm, which were slightly larger than that from the beads with immersion oil.

Considering that the 200 nm fluorescent beads exhibit better photostability, we decided to use the 200 nm beads rather than the 20 nm beads. And, we confirmed that the conclusions reported in this study are not affected by the relatively large beads.

Read noise and rSNR. As shown in Table 1, the measured read noise of the Dhyana 95 sCMOS camera working at high gain mode is comparable to Hamamatsu Flash 4.0 V2 or other mainstream sCMOS cameras, but the Dhyana 95 sCMOS camera working at low gain mode is obviously not well optimized. Not surprisingly, the Andor iXon 897 Ultra EMCCD camera exhibits a very small read noise (0.53 e–) when this camera is working at EM gain = 100. If necessary, the read

Table 1. Read noise values of the test cameras

CAMERA	WORKING MODE	READ NOISE (MANUFACTURE)	READ NOISE (MEASURED)[A]
Tucsen Dhyana 95	High gain	1.71 e– median	1.80 e– (rms) 1.71 e– (median)
	Low gain	–	41.60 e– (rms) 40.23 e– (median)
Hamamatsu Flash 4.0 V2	Camera link	1.3 e–	1.45 e– (rms) 1.14 e– (median)
Andor iXon 897 Ultra	EM gain = 100	0.51 e–	0.53 e– (rms)

[a]rms is the abbreviation for root mean square.

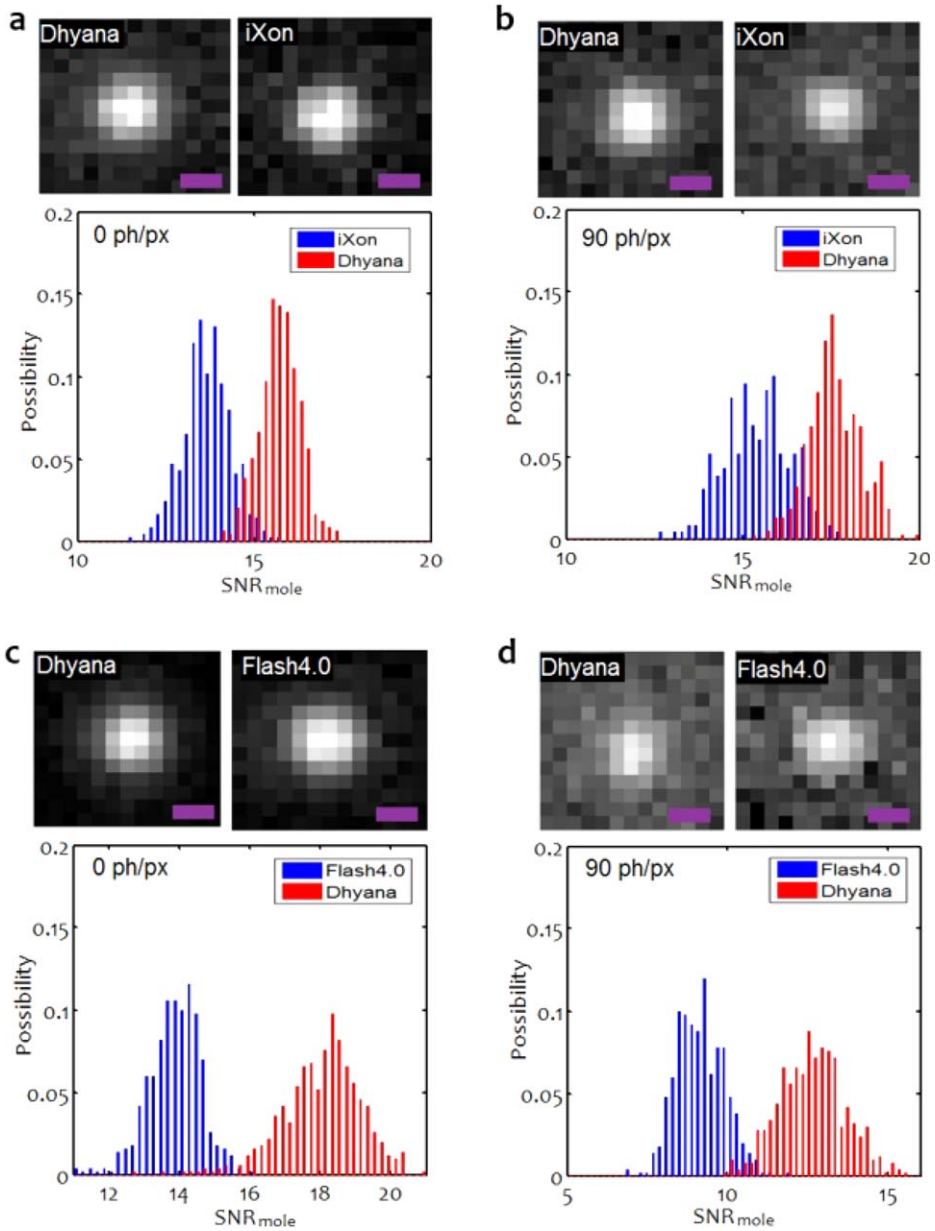

Figure 6. Direct experimental comparison of the tested cameras using raw fluorescence images from the same beads under different photon background levels. (a) Dhyana 95 (upper-left) versus iXon 897 Ultra (upper-right) at 0 ph/px background. (b) Dhyana 95 (upper-left) versus iXon 897 Ultra (upper-right) at 90 ph/px background. (c) Dhyana 95 (upper-left) and Flash 4.0 V2 (upper-right) at 0 ph/px background. (d) Dhyana 95 (upper-left) and Flash 4.0 V2 (upper-right) at 90 ph/px background. The histograms in the bottom of (a-d) shows the distribution of the SNR_{mole}. For each comparison, a total of 500 raw images were acquired synchronously from the same beads. Scale bar: 300 nm. [Color figure can be viewed at wileyonlinelibrary.com]

noise of the EMCCD camera could be even smaller when a higher EM gain is used.

From the PTC measurements, we can also calculate the rSNR curves of the test cameras working at different modes (Fig. 5). Note that rSNR was measured at uniform light, so the signal in Figure 5 denotes mean incident signal (photon per pixel, ph/px). The comparison results between Tucsen Dhyana 95 and Hamamatsu Flash 4.0 V2 or Andor iXon 897 Ultra at single pixel level are shown in Fig. 5: 1) the Tucsen Dhyana 95 at high gain mode presents much better rSNR than the Hamamatsu Flash 4.0 V2 when the signal is below 1500 ph/px; 2) the Tucsen Dhyana 95 at high gain mode presents much better rSNR than the Andor iXon 897 Ultra when the signal is above 4 ph/px; 3) However, the rSNR values of the Tucsen Dhyana 95 at low gain mode is surprisingly smaller than those from the Hamamatsu Flash 4.0 V2/Andor iXon 897 Ultra, indicating that the read noise of the Tucsen Dhyana 95 at low gain mode requires a better optimization. Therefore, the Tucsen Dhyana 95 camera is used at high gain mode in this article unless otherwise specified. Additionally, the Tucsen

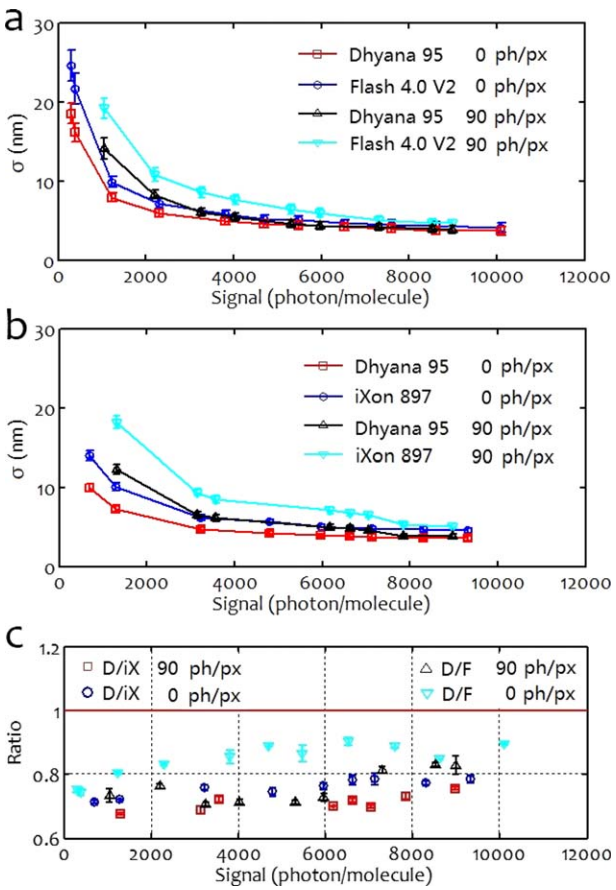

Figure 7. Direct experimental comparison on the localization precision (σ) of the test cameras under two photon background levels (shown in the inset of the figures). (**a**) Dhyana 95 versus Flash 4.0 V2. (**b**) Dhyana 95 versus iXon 897 Ultra. (**c**) Relative localization precision between the Dhyana 95 and the Flash 4.0 V2 or the iXon 897 Ultra. D is for Dhyana 95, iX is for iXon 897 Ultra, and F is for Flash 4.0 V2, respectively. The ratio is defined as σDhyana 95/σiXon 897 or σDhyana 95/σFlash4.0V2, thus the Dhyana 95 camera presents better localization precision if the ratio is < 1. The error bars indicate the standard deviation from 40 subsets. The red line in (c) was drawn to guide viewing. [Color figure can be viewed at wileyonlinelibrary.com]

Dhyana 95 at high gain mode is close to a shot-noise-limit camera with 95% QE in a wide signal range (approximately 50–1000 ph/px), while the Andor iXon 897 Ultra is never close to a shot-noise-limited camera with 97% QE due to the unavoidable excess noise from the electron-multiplying process.

Direct Comparison of the Imaging Performance between the Dhyana 95 Camera and the Flash 4.0 V2 or the iXon 897 Ultra Cameras

A direct comparison between the Dhyana 95 camera and the Flash 4.0 V2 camera or the iXon 897 Ultra camera would be helpful for understanding the imaging performance of the new 95% QE sCMOS camera. Here, the total incident signal was controlled to range from 300 to 10000 photons per molecule, covering the typical signal range for fluorescence proteins and chemical probes used in SRLM (25). Meanwhile, we selected two photon background levels with a mean value of 0 and 90 ph/px to represent extremely low and high photon background, respectively.

SNR is a popular parameter for quantifying image quality. Therefore, we firstly compared the imaging performance of the tested cameras using SNR from each molecule ($SNR_{mole} = S_{peak}/sqrt[\alpha(S_{peak} + \sigma^2_{bkg})]$). Here the peak signal (S_{peak}) is calculated from the amplitude of Gaussian function, and the background fluctuation ($\sigma^2_{bkg,}$ variance) is calculated from the pixels surrounding (typically two pixels away) the signal regions. α is used for compensating the splitting ratio difference ($\alpha = 1$ for Dhyana 95, and 0.92 for both iXon 897 and Flash 4.0V2). Experimentally, we captured a total of 500 paired raw images from the same fluorescence beads using two tested cameras, and then performed statistic analysis on the SNR_{mole}. We found that, for all the tested scenarios, the Dhyana 95 exhibits higher SNR_{mole} than its competitors: 15.7 ± 0.6 (Dhyana 95) versus 13.6 ± 0.6 (iXon 897) (Fig. 6a), 17.6 ± 0.8 (Dhyana 95) versus 15.4 ± 0.9 (iXon 897) (Fig. 6b),

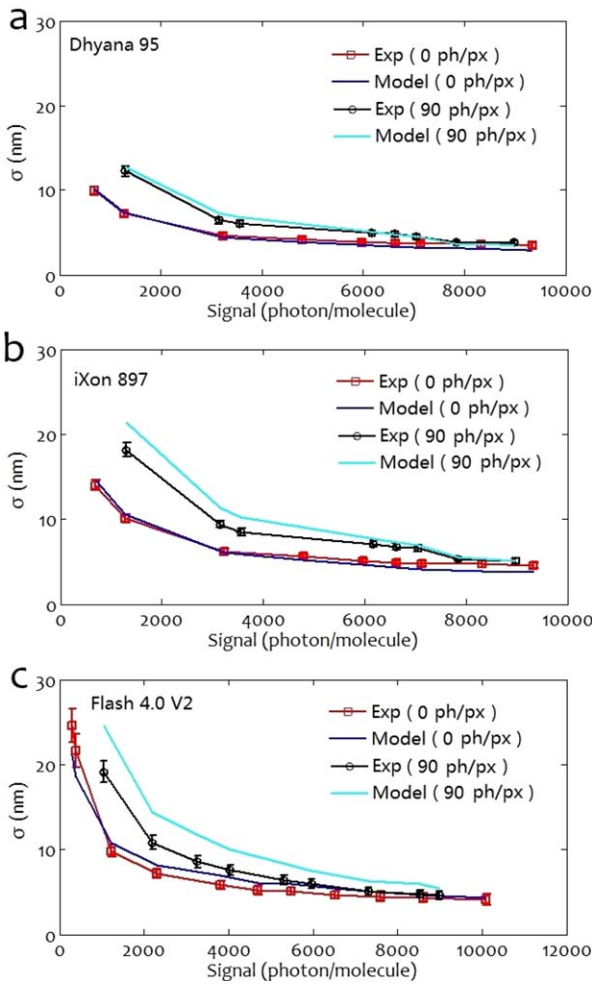

Figure 8. Comparing experimental and modeled localization precision for the Dhyana 95 (**a**), the iXon 897 Ultra (**b**), and the Flash 4.0 V2 (**c**) at two photon background levels. The error bars indicate the standard deviation from 40 subsets. [Color figure can be viewed at wileyonlinelibrary.com]

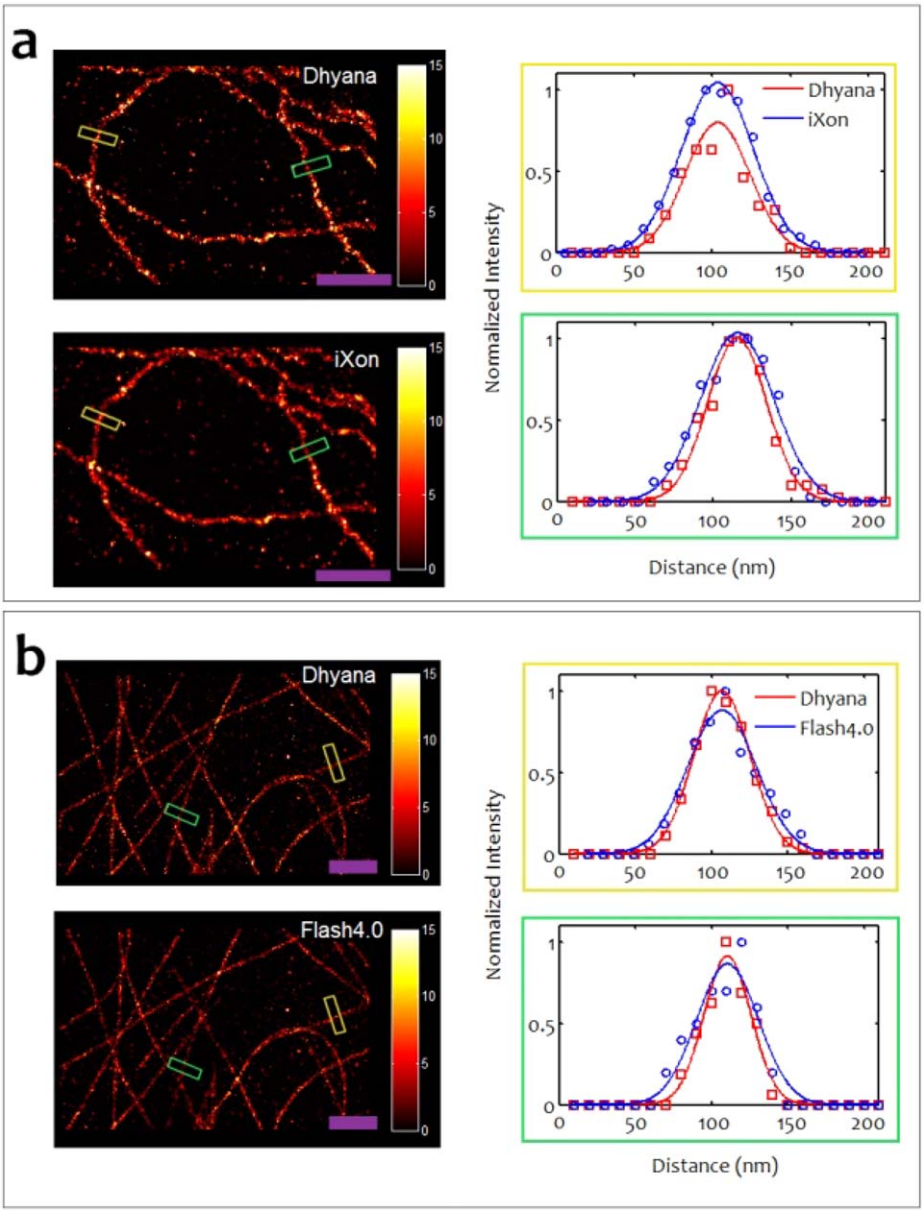

Figure 9. Direct experimental comparison on cell imaging using the tested cameras. (**a**) Dhyana 95 (upper-left) versus iXon 897 Ultra (lower-left). (**b**) Dhyana 95 (upper-left) versus Flash 4.0 V2 (lower-left). Each localization is rendered as a Gaussian with a standard deviation equal to its localization precision. The boxed areas in (a) and (b) were used to generate the corresponding cross-sectional distribution showed in the right panels. The data were fitted with Gaussian function to calculate FWHM. A smaller FWHM indicates a better spatial resolution. Scale bar: 1 μm. [Color figure can be viewed at wileyonlinelibrary.com]

18.0 ± 1.1 (Dhyana 95) versus 13.8 ± 0.8 (Flash 4.0 V2) (Fig. 6c), and 12.6 ± 1.0 (Dhyana 95) versus 9.1 ± 0.7 (Flash 4.0 V2) (Fig. 6d). The higher SNR_{mole} from the Dhyana 95 camera indicates that this camera has better imaging performance than the iXon 897 Ultra camera and the Flash 4.0 V2 camera.

We further compared the localization performance between the Dhyana 95 and the Flash 4.0 V2 or the iXon 897 Ultra. We found that the Dhyana 95 provides better localization precision than the Flash 4.0 V2 or the iXon 897 Ultra at all of the signal levels in this study (that is, 300–10000 photon/molecule in total signal), and that the superiority of the Dhyana 95 over the Flash 4.0 V2 or the iXon 897 Ultra is even more obvious when the photon background is high (see Fig. 7a–c, 90 ph/px). Therefore, we conclude that the Dhyana 95 sCMOS camera is a highly competitive sCMOS camera to be used in SRLM in a wide signal range (300–10000 photon/molecule).

Comparing Localization Precision: Experimental versus Modeled

Finally, we calculated the modeled localization precision using the formulas reported in reference 16 (see Eq. 1) and

reference 11 (see Eq. 2), where the parameters were all defined in those papers and were set here to be the same as the experiments.

$$\sigma_{sCMOS} = \sqrt{2\frac{\sigma_a}{N}\left(\frac{16}{9} + \frac{8\pi{\sigma_a}^2 b^2}{Na^2}\right)} \quad (1)$$

$$\sigma_{EMCCD} = \sqrt{2\left(\frac{2s^2 + {a^2}/{12}}{\psi N} + \frac{16\pi s^4 b}{a^2(\psi N)^2}\right)} \quad (2)$$

As shown in Figure 8, the modeled localization precision results are close to the experimental results for all of the test cameras. However, the gap between the experimental and the modeled localization precision is visible when the cameras are working at high photon background (90 ph/px), especially for the Flash 4.0 V2 and the iXon 897 Ultra. This gap may be due to the fact that the maximum likelihood estimator used in this study (MaLiang (19)) tends to overestimate the PSF sigma in the case of high photon background.

Direct Comparison of the STORM Images between the Dhyana 95 Camera and the Flash 4.0 V2 or the iXon 897 Ultra Cameras

We used STORM images of microtubulins to evaluate the imaging performance of the Dhyana 95 camera. The optical setup was described in "Optical Setup for Direct Comparison of Two Low-Light Cameras" Section. A total of 10,000 raw images was used to reconstruct a STORM image. We performed cross-sectional distribution analysis on the STORM images and calculated the FWHM of each line. We found that the Dhyana 95 camera provides smaller FWHM (thus better resolution) than the iXon 897 or the Flash 4.0V2 cameras: 48 nm (Dhyana 95) versus 54 nm (iXon 897) (Fig. 9a, upper-right), 44 nm (Dhyana 95) versus 55 nm (iXon 897) (Fig. 9a, lower-right), 44 nm (Dhyana 95) versus 53 nm (Flash 4.0 V2) (Fig. 9b, upper-right), and 37 nm (Dhyana 95) versus 48 nm (Flash 4.0 V2) (Fig. 9b, lower-right). These results are consistent with the molecular SNR results shown in "Direct Comparison of the Imaging Performance between the Dhyana 95 Camera and the Flash 4.0 V2 or the iXon 897 Ultra Cameras" Section.

Discussion

In this article, we present a methodology for directly comparing the imaging performance of two cameras under almost identical experimental conditions. Based on this methodology, we performed a detailed characterization on the imaging performance of a newly released back-illuminated 95% QE sCMOS camera called Tucsen Dhyana 95. The characterization is based on PTC measurement datasets and the paired experimental datasets between Dhyana 95 and a representative front-illuminated 72% QE sCMOS camera (Hamamatsu Flash 4.0 V2) and a popular back-illuminated 97% QE EMCCD camera (Andor iXon 897 Ultra). We found that the Tucsen Dhyana 95 presents better sensitivity (according to PTC rSNR results) and localization performance (according to the direct experimental localization precision and resolution comparison results) than a representative front-illuminated 72% QE sCMOS camera (Hamamatsu Flash 4.0 V2) and a popular back-illuminated 97% QE EMCCD camera (Andor iXon 897 Ultra), in a signal range (300–10,000 photon/molecule). This range is broad enough to cover nearly all fluorescence proteins (emit typically 400–1200 photon/molecule) and chemical probes (emit typically 1000–8000 photon/molecule) used in SRLM. Based on the results in this study, we conclude that back-illuminated 95% QE sCMOS cameras have great potential to be the best camera to be used in most SRLM applications.

Literature Cited

1. Betzig E, Patterson GH, Sougrat R, Lindwasser OW, Olenych S, Bonifacino JS, Davidson MW, Lippincott-Schwartz J, Hess HF. Imaging intracellular fluorescent proteins at nanometer resolution. Science 2006;313:1642–1645.
2. Hess ST, Girirajan TPK, Mason MD. Ultra-high resolution imaging by fluorescence photoactivation localization microscopy. Biophys J 2006;91:4258–4272.
3. Rust MJ, Bates M, Zhuang X. Stochastic optical reconstruction microscopy (STORM) provides sub-diffraction-limit image resolution. Nat Methods 2006;3: 793–795.
4. Heilemann M, van de Linde S, Schüttpelz M, Kasper R, Seefeldt B, Mukherjee A, Tinnefeld P, Sauer M. Subdiffraction-resolution fluorescence imaging with conventional fluorescent probes. Angew Chem Int Ed 2008;47:6172–6176.
5. Gould TJ, Verkhusha VV, Hess ST. Imaging biological structures with fluorescence photoactivation localization microscopy. Nat Protoc 2009;4:291–308.
6. van de Linde S, Löschberger A, Klein T, Heidbreder M, Wolter S, Heilemann M, Sauer M. Direct stochastic optical reconstruction microscopy with standard fluorescent probes. Nat Protoc 2011;6:991–1009.
7. Sengupta P, Van Engelenburg SB, Lippincott-Schwartz J. Superresolution imaging of biological systems using photoactivated localization microscopy. Chem Rev 2014; 114:3189–3202.
8. Small A, Stahlheber S. Fluorophore localization algorithms for super-resolution microscopy. Nat Methods 2014;11:267–279.
9. Janesick JR. Photon transfer. San Jose: SPIE Press; 2007.
10. Long F, Zeng S, Huang ZL. Localization-based super-resolution microscopy with an sCMOS camera Part II: Experimental methodology for comparing sCMOS with EMCCD cameras. Opt Express 2012;20:17741–17759.
11. Quan T, Zeng S, Huang ZL. Localization capability and limitation of electron-multiplying charge-coupled, scientific complementary metal-oxide semiconductor, and charge-coupled devices for superresolution imaging. J Biomed Opt 2010;15: 066005-066005–066006.
12. Huang Z-L, Zhu H, Long F, Ma H, Qin L, Liu Y, Ding J, Zhang Z, Luo Q, Zeng S, et al. Localization-based super-resolution microscopy with an sCMOS camera. Opt Express 2011;19:19156–19168.
13. Saurabh S, Maji S, Bruchez MP. Evaluation of sCMOS cameras for detection and localization of single Cy5 molecules. Opt Express 2012;20:7338–7349.
14. Huang F, Hartwich TMP, Rivera-Molina FE, Lin Y, Duim WC, Long JJ, Uchil PD, Myers JR, Baird MA, Mothes W, et al. Video-rate nanoscopy using sCMOS camera-specific single-molecule localization algorithms. Nat Methods 2013;10:653–658.
15. Deschout H, Zanacchi FC, Mlodzianoski M, Diaspro A, Bewersdorf J, Hess ST, Braeckmans K. Precisely and accurately localizing single emitters in fluorescence microscopy. Nat Methods 2014;11:253–266.
16. Mortensen KI, Churchman LS, Spudich JA, Flyvbjerg H. Optimized localization analysis for single-molecule tracking and super-resolution microscopy. Nat Methods 2010;7:377–381.
17. Long F, Zeng SQ, Huang ZL. Effects of fixed pattern noise on single molecule localization microscopy. Phys Chem Chem Phys 2014;16:21586–21594.
18. Abraham AV, Ram S, Chao J, Ward ES, Ober RJ. Quantitative study of single molecule location estimation techniques. Opt Express 2009;17:23352–23373.
19. Quan T, Li P, Long F, Zeng S, Luo Q, Hedde PN, Nienhaus GU, Huang Z-L. Ultra-fast, high-precision image analysis for localization-based super resolution microscopy. Opt Express 2010;18:11867–11876.
20. Smith CS, Joseph N, Rieger B, Lidke KA. Fast, single-molecule localization that achieves theoretically minimum uncertainty. Nat Methods 2010;7:373–375.
21. Chao J, Ward ES, Ober RJ. Fisher information for EMCCD imaging with application to single molecule microscopy// Conference on Signals, Systems and Computers (ASILOMAR), 2010 Conference Record of the Forty Fourth Asilomar. Pacific Grove, CA: IEEE; 2010. pp. 1085–1089.
22. Chao J, Ram S, Ward ES, Ober RJ. Ultrahigh accuracy imaging modality for super-localization microscopy. Nat Methods 2013;10:335–338.
23. Li L, Li M, Zhang Z, Huang Z-L. Assessing low-light cameras with photon transfer curve method. J Innov Opt Health Sci 2016;09:1630008-1630008–1630017.
24. EMVA 1288 standard release 3.1, European Machine Vision Association. Available at http://www.emva.org/.
25. Jones SA, Shim S-H, He J, Zhuang X. Fast, three-dimensional super-resolution imaging of live cells. Nat Methods 2011;8:499–505.